

# Dynamically tunable plasmonically induced transparency by planar hybrid metamaterial

Xiaoyang Duan,<sup>1</sup> Shuqi Chen,<sup>1,\*</sup> Hua Cheng,<sup>1</sup> Zhancheng Li,<sup>1</sup> and Jianguo Tian<sup>1,2</sup>

<sup>1</sup>The Key Laboratory of Weak Light Nonlinear Photonics, Ministry of Education, School of Physics and TEDA Applied Physics School, Nankai University, Tianjin 300457, China

<sup>2</sup>e-mail: jjtian@nankai.edu.cn

\*Corresponding author: schen@nankai.edu.cn

Received November 20, 2012; revised December 22, 2012; accepted January 11, 2013;  
posted January 14, 2013 (Doc. ID 180302); published February 8, 2013

We design and numerically analyze a dynamically tunable, plasmonically induced transparency (PIT) planar hybrid metamaterial (MM) in a near-infrared regime, which combines the near-field coupling effect into dynamic MM. The embedded position of tunable material in dynamic MM is optimized. Thermal-tunable VO<sub>2</sub> stripes are filled in the cut-out slots as components of a plasmonic system, which dramatically improve the dynamic modulation depth of the PIT. We also present a four-level plasmonic system to quantitatively analyze the dynamically tunable PIT device. This work may offer a further step in the design of the tunable PIT effect. © 2013 Optical Society of America  
OCIS codes: 160.3918, 240.6680, 230.4555.

As one of the most fascinating near-field couplings in a plasmonic system, plasmonically induced transparency (PIT) in metamaterials (MMs) mimics the quantum interference effect of electromagnetic induced transparency (EIT) in laser-driven atomic systems, which gives rise to the narrow transparency window within a broad transmission dip [1,2]. PIT lays the foundation of manipulating light by employing metal nanostructures as the effective media with EIT-like optical properties, which underlies many useful applications, such as slow light [3], plasmonic sensing [4], and optical switching [5]. In spite of obvious advantages of room-temperature manipulability, artificially controlling spectral response and the ability to integrate with nanoplasmonic circuits, the previous designed PIT devices principally have an inherent drawback. The transparent window of PIT has to be tuned by accurately modifying the structure, which needs to fabricate many different PIT devices.

Recently, a number of studies have focused on dynamic control of the MM resonance, since it can help to overcome some limitations of custom designs [6–9]. The dynamic MM resonance can be formed by incorporating tunable-materials, such as semiconductor [6], superconductor [7], and oxide films [8,9]. However, previously designed dynamic MMs are composed of arrays of metal resonators printed on tunable materials substrates, so the dynamic response can only be realized by tuning the optical properties of the substrates rather than the plasmonic system itself, which inevitably results in a low modulation depth. Therefore, the embedded position of tunable material should be further optimized to obtain a high modulation depth. In addition, there has recently been increasing interest in MMs based on VO<sub>2</sub> phase transition due to the following facts: (i) tunability at room temperature, (ii) simple processability and controllability, (iii) easy to integrate with nanoplasmonic circuits, (iv) drastic conductivity change in near-infrared [9,10].

In this Letter, we propose the design and analysis of a dynamically tunable PIT planar hybrid MM in a

near-infrared regime, in which VO<sub>2</sub> stripes are filled in the cut-out slots as components of a plasmonic system. Results show that the PIT effect of the hybrid MM can be agilely tuned by adjusting the temperature of VO<sub>2</sub> stripes without modifying the structure accurately. This special embedded position of VO<sub>2</sub> stripes will dramatically improve the dynamic modulation depth. Meanwhile, a four-level plasmonic system is employed to explain the PIT feature quantitatively, and the results agree well with the simulated results.

Most studies show that introducing an asymmetry to the spatial arrangement is a prerequisite for PIT [11], since the asymmetry permits excitation of the otherwise forbidden dark mode. We proposed a local asymmetrical but whole rotational symmetrical nanostructure. The designed tunable PIT device consists of three layers: a metallic plane layer on the bottom, a dielectric layer, and finally, a second metallic layer on the top, as shown in Fig. 1. It is fabricated on a quartz substrate with permittivity of 2.25. The two metallic layers are separated by a 0.15 μm thick Al<sub>2</sub>O<sub>3</sub> with dielectric constant and loss tangent as 2.28 and 0.04 [12]. The optical constants of gold in an infrared regime are described by the Drude model

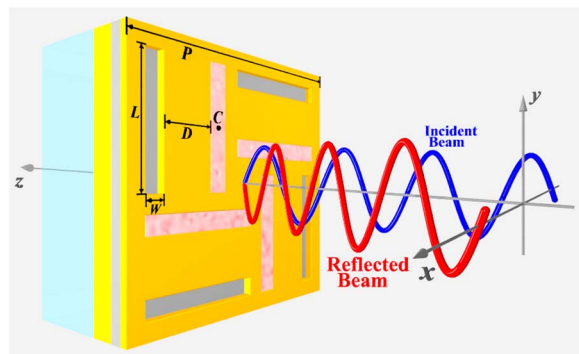


Fig. 1. (Color online) Unit cell of the designed tunable PIT device showing the geometry parameters:  $P = 3.0 \mu\text{m}$ ,  $L = 1.4 \mu\text{m}$ ,  $W = 0.2 \mu\text{m}$ ,  $D = 0.6 \mu\text{m}$ . The coordinate of the inner VO<sub>2</sub> strip is  $C(400, 600) \text{nm}$ .

[13]. The top layer consists of four rotationally aligned cut-out “=” pairs and four VO<sub>2</sub> stripes. Four VO<sub>2</sub> stripes are filled in the four inner cut-out slots, which are simulated with a thermal-tunable permittivity  $\epsilon$  and conductivity  $\sigma$  [10]. The optimized structure was achieved by using the finite-element-method (FEM)-based commercial software COMSOL Multiphysics.

To analyze the dynamic response of the designed tunable PIT device, we consider that a  $y$ -polarized TEM beam is normally incident on the upper face of the tunable PIT device. The blue circled curves in Fig. 2 show the simulated, normalized reflection spectra  $R(\omega)$  for different temperatures. The PIT tuning feature is apparent in the reflection spectra, and more accurately, it is the plasmonically induced reflectance (PIR) effect [4]. The reflection is dramatically increased as the bottom metallic layer is much thicker than the penetration depth of light, which enhances the PIR effects. At first, at the temperature of 347 K, there is a broad reflection dip with a reflection minimum  $R(\omega) = 27.9\%$  at 2.99  $\mu\text{m}$ . Then, a tiny reflection peak emerges within the broad reflection dip with decreasing temperature. Finally, the reflection peak can reach  $R(\omega) = 61.2\%$  at 3.01  $\mu\text{m}$  in the case of  $T = 333$  K. A large dynamic modulation depth is obtained as VO<sub>2</sub> stripes are filled in the inner cut-out slots, which will be as components of plasmonic system with the increasing of temperature.

To gain insight into the nature of the designed tunable PIT device, we calculated the electric-field amplitude distribution and the surface-current density distribution of the top metallic layer for a  $y$ -polarized TEM wave at 3.01  $\mu\text{m}$ , as shown in Fig. 3. In the case of  $T = 347$  K, the VO<sub>2</sub> stripes can be considered a good conductor. So, only the cut-out slots parallel to  $x$  axis can be excited by the incident beam, which exhibits a strong electric field and high surface current densities [as shown in Fig. 3(a)]. It is a bright mode in the plasmonic system and suffers significant radiative losses, which supports the broad reflection dip. With the decrease of temperature, the VO<sub>2</sub> stripes are gradually forming dielectric

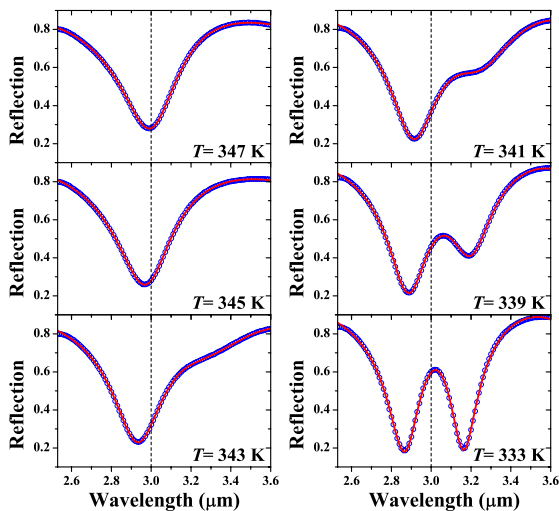


Fig. 2. (Color online) Simulated reflection spectra achieved by FEM (blue-circled curves) and four-level plasmonic system (red-solid curves) of the tunable PIT device for different temperatures.

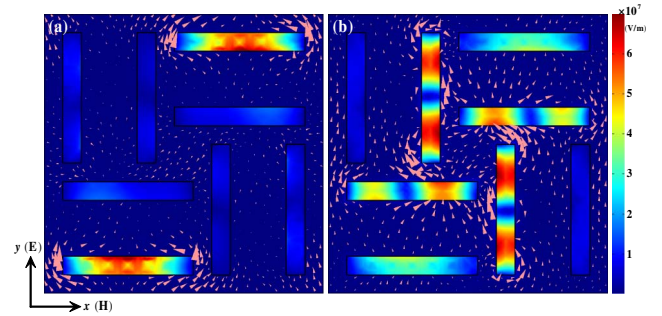


Fig. 3. (Color online) Colormaps and pink arrows, respectively, represent the distributions of the amplitude of the electric fields and induced surface current densities of the top metallic elements at 3.01  $\mu\text{m}$  for (a)  $T = 347$  K and (b)  $T = 333$  K.

stripes. The VO<sub>2</sub> stripes parallel and perpendicular to the  $y$  axis can be regarded as the dark mode and additional mode, respectively. When the temperature is decreased to  $T = 333$  K, the electric field and surface current are strongly coupled back to the dark mode, leading to a destructive interference and a suppressed state in the bright mode. Thus, the dark mode is excited where it has a strong electric field and surface current distribution, and the electric field and surface current of the bright mode decrease greatly [as shown in Fig. 3(b)]. Meanwhile, the additional mode shares a small part of the dark mode energy due to near-field coupling. In fact, it is the decrease of conductivity that gradually stimulates the excitation of the PIT effect via the coupling among the bright, dark, and additional modes, which leads to a narrow reflection peak in the broad dip.

To provide a quantitative description, we proposed a four-level plasmonic system to explain the forming mechanisms of the tunable PIT device in Fig. 4(a). The

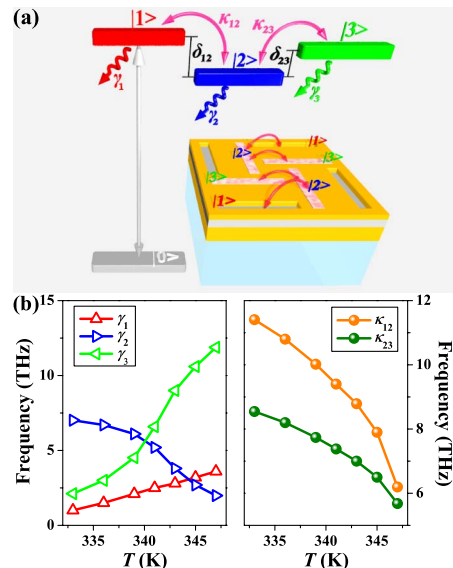


Fig. 4. (Color online) (a) Coupled four-level plasmonic system for the tunable PIT device. The pink arrows on the unit cell indicate the near-field coupling between meta-atoms. (b) Extracted simulated coupling and damping parameters as a function of temperature. Values of  $\gamma_1$ ,  $\gamma_2$ ,  $\gamma_3$ ,  $\kappa_{12}$ , and  $\kappa_{23}$  are extracted by fitting the simulated reflection spectra.

system consists of three artificial modes, a radiative plasmonic state  $|1\rangle = \tilde{A}_1(\omega)e^{i\omega t}$  (bright mode), a dark plasmonic state  $|2\rangle = \tilde{A}_2(\omega)e^{i\omega t}$  (dark mode), and an additional plasmonic state  $|3\rangle = \tilde{A}_3(\omega)e^{i\omega t}$  (additional mode), which have resonant frequencies  $\omega_{01}$ ,  $\omega_{02}$ ,  $\omega_{03}$ , and damping factors  $\gamma_1$ ,  $\gamma_2$ ,  $\gamma_3$ , respectively. A four-level plasmonic system is formed by three states of coupled meta-atoms and a continuum state (ground state  $|0\rangle$ ). We assume that the dark mode does not couple with the external field, while geometrical parameters  $g_1$ ,  $g_3$  indicate how strongly the bright mode and additional mode couple with the external field  $E_0 = \tilde{E}_0 e^{i\omega t}$ . Then, the field amplitude of all states can be described as a system of linearly coupled Lorentzian oscillators:

$$\begin{bmatrix} \omega - \omega_{01} + i\gamma_1 & \kappa_{12} & 0 \\ \kappa_{12} & \omega - \omega_{02} + i\gamma_2 & \kappa_{23} \\ 0 & \kappa_{23} & \omega - \omega_{03} + i\gamma_3 \end{bmatrix} \times \begin{bmatrix} \tilde{A}_1 \\ \tilde{A}_2 \\ \tilde{A}_3 \end{bmatrix} = - \begin{bmatrix} g_1 \tilde{E}_0 \\ 0 \\ g_3 \tilde{E}_0 \end{bmatrix}. \quad (1)$$

Corresponding to the geometric position of the modes, we define  $\kappa_{12}$  as the coupling parameter between  $|1\rangle$  and  $|2\rangle$ , and  $\kappa_{23}$  as the coupling parameter between  $|2\rangle$  and  $|3\rangle$ . The near-field coupling between  $|1\rangle$  and  $|3\rangle$  is ignored due to the far distance. In Eq. (1), the complex amplitude of the bright mode  $\tilde{A}_1$  is directly proportional to the polarizability of the plasmonic system. Therefore, the normalized absorption  $A(\omega)$  is obtained as  $A(\omega) = |\tilde{A}_1|/|\tilde{E}_0|$ , and the reflection is  $R(\omega) = 1 - A(\omega)$ . Figure 2 also shows the simulated reflection spectra at different temperatures. The close agreement between this analytical derivation and the FEM analysis confirms the validity of our design.

To examine the coupling and damping parameters of our four-level plasmonic system, Fig. 4(b) shows the fitting values of  $\gamma_1$ ,  $\gamma_2$ ,  $\gamma_3$ ,  $\kappa_{12}$ , and  $\kappa_{23}$  as a function of temperature in frequency units. The resonant frequencies of the mode are approximately  $\omega_{01} = 96$  THz,  $\omega_{02} = 85$  THz and  $\omega_{03} = 93$  THz, respectively. We define  $\delta_{12} = \omega_{01} - \omega_{02}$  and  $\delta_{23} = \omega_{02} - \omega_{03}$  as the small detuning. The increasing of the damping factor  $\gamma_2$  corresponds to the emerging and narrowing of the transmission peak. The change of damping factor  $\gamma_1$  is small at different temperatures as the bright mode is hardly affected by the temperature. With the decreasing of temperature, damping factor  $\gamma_3$  is gradually close to  $\gamma_1$  as the additional mode is gradually similar to the bright mode.

Significantly,  $\kappa_{12}$  is approximately inversely proportional to temperature, which determines the modulation strength of our tunable PIT device. With the decreasing of temperature, the dark and additional modes appear, and the near-field coupling  $\kappa_{23}$  is also increasing. Such quantitative results confirm our expectation about the relationship between the thermal-tunable conductivity and coupling strength of meta-atoms.

In conclusion, we have numerically analyzed a dynamically tunable PIT planar hybrid MM based on coupled meta-atoms. The near-field coupling PIT effect can be extended into the hybrid MMs by optimizing the embedded position of tunable material. This not only dramatically improves the dynamic modulation depth, but also does not need to modify the structure accurately. The provided analytical investigations are kept general and so can be easily extended to other antenna geometries. Our proposed dynamic planar hybrid MMs may offer a further step forward in the design of tunable PIT effect and the capability of optical modulation.

This work was supported by the CNKBRFSF (2011CB922003), the 973 Program (2012CB921900), the NSFC (61008002), and the SRFDP (20100031120005 and 20120031120032).

## References

1. S. Zhang, D. A. Genov, Y. Wang, M. Liu, and X. Zhang, *Phys. Rev. Lett.* **101**, 047401 (2008).
2. N. Liu, L. Langguth, T. Weiss, J. Kästel, M. Fleischhauer, T. Pfau, and H. Giessen, *Nat. Mater.* **8**, 758 (2009).
3. B. Tang, L. Dai, and C. Jiang, *Opt. Express* **19**, 628 (2011).
4. N. Liu, T. Weiss, M. Mesch, L. Langguth, U. Eigenthaler, M. Hirscher, C. Sönnichsen, and H. Giessen, *Nano Lett.* **10**, 1103 (2010).
5. J. Chen, P. Wang, C. Chen, Y. Lu, H. Ming, and Q. Zhan, *Opt. Express* **19**, 5970 (2011).
6. H.-T. Chen, J. F. O'Hara, A. K. Azad, A. J. Taylor, R. D. Averitt, D. B. Shrekenhamer, and W. J. Padilla, *Nat. Photonics* **2**, 295 (2008).
7. H.-T. Chen, H. Yang, R. Singh, J. F. O'Hara, A. K. Azad, S. A. Trugman, Q. X. Jia, and A. J. Taylor, *Phys. Rev. Lett.* **105**, 247402 (2010).
8. R. Singh, A. K. Azad, Q. X. Jia, A. J. Taylor, and H.-T. Chen, *Opt. Lett.* **36**, 1230 (2011).
9. W. Huang, X. Yin, C. Huang, Q. Wang, T. Miao, and Y. Zhu, *Appl. Phys. Lett.* **96**, 261908 (2010).
10. H. S. Choi, J. S. Ahn, J. H. Jung, and T. W. Noh, *Phys. Rev. B* **54**, 4621 (1996).
11. Z.-G. Dong, H. Liu, M.-X. Xu, T. Li, S.-M. Wang, J.-X. Cao, S.-N. Zhu, and X. Zhang, *Opt. Express* **18**, 22412 (2010).
12. X. Liu, T. Starr, A. F. Starr, and W. J. Padilla, *Phys. Rev. Lett.* **104**, 207403 (2010).
13. M. A. Ordal, L. L. Long, R. J. Bell, S. E. Bell, R. R. Bell, R. W. Alexander, Jr., and C. A. Ward, *Appl. Opt.* **22**, 1099 (1983).